Accelerated testing of soft soldered, small-diameter, thin-walled CuNi pipes subjected to cyclic internal pressure loading

Sophie A.M. McNair [a,b,*], Kamil Cichy [c], Jerome Daguin [c], Antti Onnela [c], Alexander J.G. Lunt [a]

[a] Department of Mechanical Engineering, The University of Bath, Claverton Down, Bath, BA2 7AY, UK
[b] Department of Design, Manufacturing and Engineering Management, The University of Strathclyde, James Weir Building, 75 Montrose Street, Glasgow, G1 1XJ, UK
[c] CERN, Geneva, Switzerland

ARTICLE INFO

ABSTRACT

Small-diameter, thin-walled pipes have applications in a wide range of industries including high-energy physics, heat transfer, nuclear, medical and communications. However, there are currently no standards that exist for permanently joining these components either via welding (melting the base material) or soldering. As such it is difficult to determine the likely performance of a thin-walled pipe connection. Porosity is largely inevitable in soldered joints and is a determining factor in the performance of a connection.

This study focused on characterisation of failure initiation and propagation within soft soldered CuNi thin-walled pipe joints under cyclic internal pressure loading. A step-stress accelerated life testing regime (SSALT) was developed to simulate the loads the joints would experience over their operational lifetime, in a shorter timescale.

10 soldered joints were studied in total, with varying levels of porosity within the soldered joints prior to testing. Pressurised Nitrogen gas was used to internally pressurise the samples, with cyclic loading between atmospheric conditions and a prescribed maximum pressure value.

The results of the SSALT showed that the soldered samples experienced early failure through crack initiation and propagation through the solder. Cracks, or failures, were seen to initiate from existing voids, or porosity, within the soft-soldered joints.

From this work, it can be concluded that the performance of soft-soldered joints under cyclic, internal pressure loading is strongly influenced by the presence of voids that are created during the manufacture of such soldered connections.

1. Introduction

Small-diameter, thin-walled, metallic tubes, or pipes, are defined as having a typical diameter less than 20 mm and a ratio of outer diameter to wall thickness of 20 and above [1]. The use of such components has increased dramatically over recent years due to advances in manufacturing techniques. They have become a key value-adding factor in a number of industries such as: particle physics, nuclear energy generation, medical science and mobile communications by allowing the production of smaller components and supporting tighter tolerances [2–5]. However, many applications of such thin-walled pipes require the use of piping longer than can be manufactured, or connection with other components of differing diameters or materials [6]. Therefore, joining thin-walled pipes is commonly required, and strong, reliable joints are crucial for the uptake of thin-walled pipes within industry.

Fusion welding is defined as a permanent connection where external heat is added, to induce melting and achieve a bond between two parts, examples include gas tungsten arc welding and laser beam welding [7, 8]. In contrast soft soldering is a solid-state welding process in which the substrate materials remain solid, but the filler material melts to produce a bond [9–11]. Both of these joining methods are well-established for numerous geometries, including metallic pipework.

Research into design and optimisation of effective joining techniques for small-diameter, thin-walled pipework is in the early stages of development, with industrial standards focused on pipe joints with a minimum sleeved connections with a filler material thickness of 0.5 mm

[12–14]. This resulting geometry is primarily relevant to materials within thin wall thicknesses as the joint strength typically must be higher than that of the substrate materials. Previous work has indicated that soft soldering can be an effective joining method for welding pipes where joints have a thickness less than 0.5 mm [15]. This work showed that residual stresses induced by heat input during the soldering process [16] had a greater impact on crack initiation and propagation than moderate levels of porosity within the soldered joint [15]. However, this work focused on tensile load cases. In operation small-diameter piping is likely to experience a range of different load cases, and as such it is important to understand the behaviour of soldered joints for different kinds of loading.

Across many industries, internal pressurisation of piping is a common use case and a primary parameter in piping design [17–20]. In many cases pressure cycling occurs in normal operation of pipelines [21]. Such cycling of internal pressure can induce early failures within piping due to fatigue failures [22] particularly where flaws in the pipeline act as stress concentrators [23,24]. In welded pipelines, defects within the weld joint such as areas of residual stress or weld cracks can drastically reduce the fatigue life of the joint when subjected to internal pressure loading [25]. Changes to the material microstructure caused by the welding process can also influence the performance of welded pipelines under cyclic load conditions [26]. However, studies focused on performance of pipe welds under internal pressure loading have so far focused on weld thicknesses that are greater than 0.5 mm, with little information on the performance of welds below 0.5 mm in thickness.

This work will focus on the lifetime performance of soldered joints around 0.15 mm in thickness subjected to cyclic, internal pressure loading. To do this, a step-stress accelerated life testing regime (SSALT) was developed in accordance with the expected loading conditions the components would be subjected to in service. A SSALT is an experimental regime that tests samples to failure at stresses above expected operational stresses [27]. During a SSALT, a given stress level is held for a predetermined amount of time, after which the part is tested for failure. If no failure is apparent, the stress level is increased and held for another predetermined time. This process is repeated until the end of the predetermined test regime, or failure of the part [28].

This type of testing aims to quantify the expected performance of the part under the operation, or design, stress by accelerating time to failure using higher testing stresses. A typical SSALT stress pattern and the translation of performance under testing stresses to the 'equivalent' performance under design stresses can be seen in Fig. 1. The resulting part can then be directly analysed to assess the likely impact of the non-accelerated test on the part being analysed.

The intended application for the samples tested in this work were for
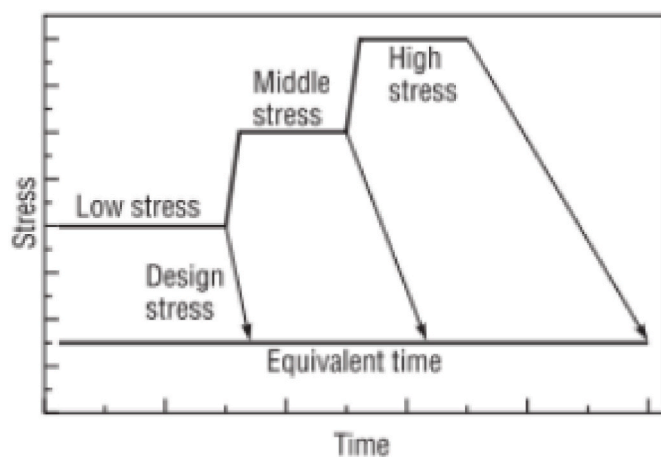
use in high energy physics detectors, namely the CMS experiment at CERN, Switzerland. The CMS experiment is undergoing a planned upgrade in detection capabilities [30], which requires an upgraded cooling system in order to maintain a tightly controlled temperature profile and maximise detector performance [31]. To do this, a two-phase CO_2 cooling system has been developed that will operate at a nominal pressure between 8 and 28 bar, with maximum pressure expected to reach 85 bar during shut down and start-up of the system. The design pressure of the system is 130 bar and burst discs rated to this pressure are included within the assembly [32]. Operational temperature is expected to be -35 °C [33,34]. The cooling channels that facilitate the transport of the CO_2 refrigerant and heat transfer from components will be small in diameter (between 2.0 and 2.5 mm outer diameter) and have thin walls (between 0.10 and 0.25 mm thickness). This geometry was selected for a number of reasons: firstly, it is advantageous to reduce the material budget of high-energy physics detectors, defined as the length of material which a particle has to traverse. By incorporating thin walls into the pipework, the overall material budget of CMS is reduced, which has a direct effect on the detection of particles generated in collisions [35–37]. Secondly, the diameter of the pipework was selected to deliver sufficient refrigerant flow at the required pressures while simultaneously promoting the two-phase flow conditions of CO_2 required to maximise heat transfer [38–41].

Although orbitally welded joints will be used in the majority of the CMS cooling system, during assembly there are a number of locations within the structure where space is severely restricted. Where space is severely restricted, several conventional joining methods cannot be used as they require ample space around the pipework for clamping, the presence of high temperatures or electric fields. Soft soldering is a solid-state joining method that can be carried out with minimal space around the area to be joined, requires only localised heating and no magnetic fields. For these reasons, soft soldering will be used in several locations within the CMS detector, and therefore characterisation of this joint type is required prior to installation.

Voids, or porosity, are an almost inevitable defect of flaw that can occur within soldered joints, caused by the heating process of the filler material [42]. During the soldering process, the application of heat can cause entrapment of gases in the molten solder, or metallisation reactions between the various materials can give rise to the formation of gases, depending upon the specific solder type, temperature or dwell period [43]. Upon solidification of the filler material, these gases cause gaps in the solder, or voids. Such voids can have a negative impact on the reliability of the soldered joint, although the impact can depend on size, shape, frequency and location [44]. Larger voids directly affect the mechanical strength of the joint due to a reduction in solder area [45], while smaller voids that exist close to one another can promote crack propagation and subsequent failure [46].

Voiding can arise from the entrapment of external gases or can result from gaseous by-products of intermetallic reactions [47]. This can lead to distinct changes to the microstructure of the joint and accordingly has been the focus of numerous solder studies, including analysis focused on the SnPbAg class of solder being used in this study [48–50]. These studies have demonstrated that higher concentrations of intermetallics can lead to increased numbers of voids, and provided a detailed overview of the chemistry and resulting atomic structure. The correlation between these effects and static joint strength has also been investigated [51] although, to the best of the authors knowledge, to date no studies have assessed the impact of voiding on the cyclic response of these types of connection.

As previously identified in the literature [15], the presence of voiding is very common for soldered connections of this type. Therefore, in order to achieve the required joint characteristics, the overlap of the soldered joint is typically extended to achieve a static strength with an appropriate safety factor. What is currently less well understood is the impact of voids of multiple sizes and distributions and their impact on the cyclic performance of this joint type. Accordingly, this work aims to

Fig. 1. Typical SSALT stress pattern and a possible translation of test time to the 'equivalent' time at design stress, adapted from [29].

characterise the performance of soldered connections under cyclic pressure loads, as will be expected during the lifetime operation of the cooling system. As such, internal pressure will be used to load the samples, and samples will be exposed to a gradual increase in internal pressure until a maximum, pre-set, value is reached, after which pressure within the sample will be reduced to 1 bar (i.e., 0 additional bar above atmospheric pressure conditions).

2. Samples

2.1. Geometry

The samples used in this study were comprised of two seamless piping components with different geometries, with a sleeve to facilitate joining between the piping components. On one side of the joint, a SS316L pipe of outer diameter (d_O) 2.30 mm and wall thickness (t_w) 0.15 mm was vacuum brazed to a CuNi sleeve. At the other side, a CuNi pipe of $d_O = 2.50$ mm and $t_w = 0.25$ mm was soft soldered to the CuNi sleeve. The soldered connection was analysed in this study and is shown in greater detail in Fig. 2. The prescribed tolerances on all measurements was 0.01 mm, and the results of the CT scans demonstrated that this was achieved in all cases.

As can be seen from Fig. 2, the overlap between the CuNi pipe and the sleeve was set as 5.30 mm, and a step machined into the sleeve to ensure this overlap was maintained. The thickness of the soldered joint was 0.10 mm. Ten joints connected in series were tested as part of one sample assembly.

Within the CMS detector cooling system, vacuum brazing is the preferred method for pipe joining as it offers a high strength, consistent production method. However, this approach requires a vacuum and a large amount of access space so can only realistically be performed on piping components prior to installation in the detector. During assembly of the different sub-elements of the detector is it necessary to form new connections with limited space available. In these cases, despite the potential for reduced strength and lack of consistency, soft soldering is the only viable option. In order to facilitate this type of connection, CuNi sleeves are initially vacuum brazed to SS316L pipes and the soldering is performed onto these sleeves. Therefore, it was decided that a representative geometry would be used in this study (Fig. 11).

2.2. Materials

As discussed in Section 3.1, the pipes tested in this study were seamless pipes, manufactured from either SS316L or CuNi 70/30. The soft soldered joint used a Sn62Pb36Ag2 filler, while the vacuum brazed connection used a Ag68.5Cu26.5Pd5 filler. A Sn62Pb36Ag2 filler was selected as it is a low flux solder that is compatible and wets effectively in CuNi joints. This low flux solder was required in order to minimise the
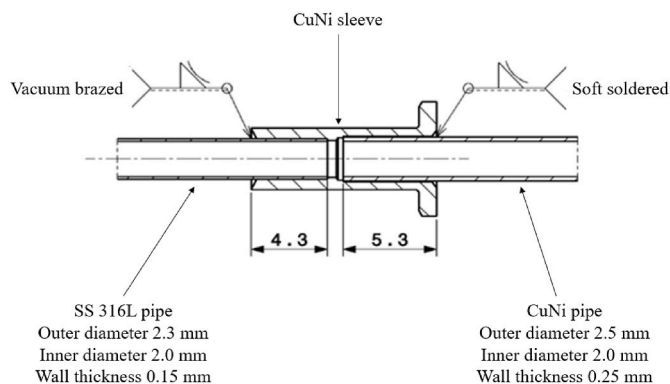
residual flux within the joint, which is known to lead to corrosion over the 10+ year expected lifetime of the cooling system.

The soft solder was applied in accordance with the manufacturer's recommended approach. This involved the use of a soldering iron which was heated to 220 °C, above the 179 °C melting point of Sn62Pb36Ag2, and held on the joint interface for 20 s. A 10 mm length of solder was then applied to the heated specimen to be drawn into the connection via capillary action. All joints were produced by an experienced technician and were compared visually prior to subsequent characterisation. For the brazed joint, the brazing temperature was 810 °C.

3. Experimental procedure

3.1. Design of step-stress accelerated life test procedure

As outlined previously, a SSALT involves inducing a constant stress configuration within a sample for a predetermined period of time, before increasing the stress gradually until failure has occurred. As part of a SSALT regime, the initial stress that the part is subjected to, S1, is higher than the normal operational stress, S0, and the part is held at this constant stress level for a set time, t1. Further stress levels, S2 – Sn, are gradually increased after the predetermined time has elapsed, Fig. 3.

The initial, lowest, testing stress, S_1, is typically designed as not to cause failure within the testing time, t_1. This prevents excess extrapolation of results and data is performed several times to increase confidence in models.

For the samples in this study, the normal operating stress, S_0, was determined to be between 8 and 28 bar internal pressure. This range of values corresponds to the pressure that the pipework will experience when the cooling system is operating at – 35 °C. This allowed for determination of the other testing stresses, as per Table 1.

The operational pressures and associated stresses on components will not exist in isolation over the 10-year lifetime of the detector. Instead, the components will experience periods of higher and lower pressures, and stresses, depending on operational conditions, hence the need to test the parts under cyclic loading conditions.

During operation the CMS detector will be pressurised for extended periods with no downtime. However, given the size and complexity of the system is highly likely that operational demands will mean that the cooling system must be shut down and depressurised to perform maintenance or repairs throughout its lifetime. Predicting the number of

Fig. 2. Vacuum brazed and soft soldered joint tested in this work showing design dimensions.
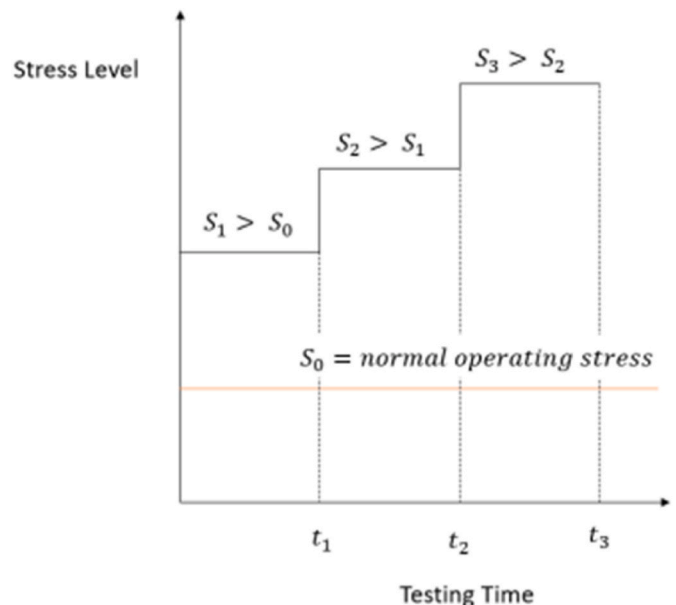
Fig. 3. Step-stress accelerated life test model.

Table 1
SSALT and corresponding relation to CMS tracker design.

Increment	Testing pressure (bar)	Number of cycles	Relation to CMS design
S_0	28	0	Expected pressure at −35 °C during operation
S_1	65	500	Minimum expected pressure at start up (from room temperature)
S_2	85	500	Maximum expected pressure at start up (from room temperature)
S_3	130	500	Design pressure - pressure at which burst discs will rupture

interventions is not trivial, as this will be the first device of this type. Therefore, in order to ascertain an estimate for the maximum number of expected cycles, a review of previous systems and extended discussion with key operation and manufacturing stakeholders was performed. This analysis provided an upper bound of 300 cycles, to which an appropriate safety factor of 1.66 was applied to select 500 as the number SSALT cycles (Table 1). Given that the minimum and maximum start up pressures are 65 bar and 85 bar respectively, these two pressures were initially selected to determine the performance under normal operation (by cycling from room pressure to these values 500 times, Fig. 4). Following this assessment, the maximum operational pressure of 130 bar was tested over 500 cycles (corresponding to the burst disk pressure) as a worst-case scenario.

As can be seen in Fig. 4, each cycle consists of several steps in which the sample is incrementally pressurised to the maximum design pressure, S_n. Once the sample has reached the maximum pressure, the pressure is held for a few seconds before the pressure is released from the sample as a rapid depressurisation to 0 bar. This cycle is repeated 500 times for each pressure increment, unless a failure is seen before this predetermined number of cycles.

3.2. Cyclic pressure testing equipment

The equipment used to carry out the cyclic pressure tests outlined in this work was a custom piece of equipment designed through a collaboration with the University of Bath and Swagelok, Bristol. The pressure test equipment was comprised of a high-pressure Nitrogen gas inlet, and a series of valves which incrementally allow the pressure within the sample to be increased. An overview of these components is outlined in Fig. 5.

As can be seen in Fig. 5, the overall system was comprised of several subsystems that perform distinct functions to facilitate the cyclic
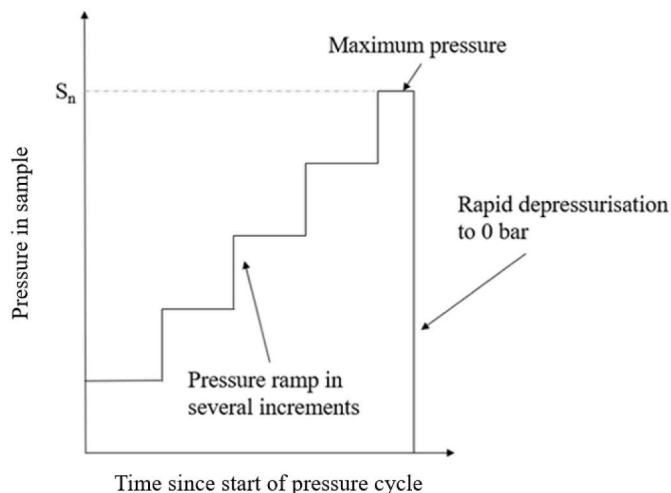
Fig. 4. Pressurisation sequence for each cycle.

pressure test process. These are Pressure Regulation, Reservoir Pressurisation, Output and Exhaust. A flow diagram describing the interactions between the different subsystems as well as the necessary inputs and outputs is described in Fig. 6, more detailed descriptions of each subsystems purpose and operation is given in Table 2.

The equipment outlined in Figs. 5 and 6 and Table 2 was controlled via a CompactDAQ (National Instruments, USA) device, which connected to an external PC. The PC then allowed for a user to change test parameters, monitor test status and save results via a specially developed LabVIEW programme (National Instruments, USA).

3.3. Analysis of samples

In order to characterise the initiation and evolution of failures within the soft soldered joints, samples were analysed using X-ray Computed Tomography (XCT) both prior to testing, and after each stress cycle had been completed i.e. after each set of 500 cycles. This was conducted using a Nikon XT H 225 ST XCT scanner (Nikon Corporation, Tokyo, Japan) using a 225 kV reflection target. For all XCT scans a source voltage of 150 kV and source power of 14.25 W were used. 1977 projection images were captured, with an exposure time of 1000 ms per image and a detector pixel size of 0.2 mm. The projections were reconstructed using the Inspect-X software (Nikon Corporation, Tokyo, Japan) and data visualisation was carried out using Avizo 9.2 (Thermo Fisher Scientific, USA).

Following all cyclic tests transverse sections of joints were taken and mounted in two part epoxy cold mounting resin (Agar Scientific, Essex, UK). Mounted samples were polished using a Struers RotoPol-11 semi-automatic grinding and polishing system (Struers, Copenhagen, Denmark). Preparation of samples was carried out based on the recommended preparation method for stainless steels by Struers [52], which can be described as follows; Plane grinding was performed using 220 grit silicon carbide sandpaper, followed by fine grinding using a 9 µm diamond abrasive. Diamond polishing was conducted using a 3 µm diamond abrasive, followed by final oxide polishing using 0.04 µm colloidal silica abrasive.

Polished cross sections were then analysed via Optical Microscopy (OM) performed using a Keyence VHX-6000 (Keyence Corporation, Osaka, Japan) microscope.

4. Results

4.1. Pre-testing analysis

Prior to testing each sample XCT was used to quantify any porosity or flaws in the solder in the 'as-delivered' condition. The results of this XCT analysis can be seen in Fig. 7.

Porosity within a soldered sample is largely unavoidable, as it is caused by the heating process of the filler material [42]. This process can cause evaporation and entrapment of gases within the solder, or gases can arise from metallisation effects between the solder material and any substrate pipe or coating material [43]. It is important to characterise any voids that exist within a sample prior to cyclic pressure testing, as voids have been shown to have a negative impact on the reliability of the joint [44].

As can be seen in Figs. 7 and 5 joints were analysed using a single XCT scan. This is due to the size of the sample, scanning a larger number of joints reduces the resolution of the XCT reconstruction, and hence smaller pores or voids may be missed. By analysing a smaller number of samples, greater detail could be obtained in the XCT reconstructions. A second XCT scan was utilised to analyse the other 5 joints.

All joints scanned prior to testing exhibited some level of porosity, with all joints containing larger pores, or voids, relative to the overall joint dimensions. For example, the joint pictured in Fig. 7a has a large, central, void with maximum outer dimension measured in 3D space of approximately 1.5 mm, which is around 58 % of the thickness of the
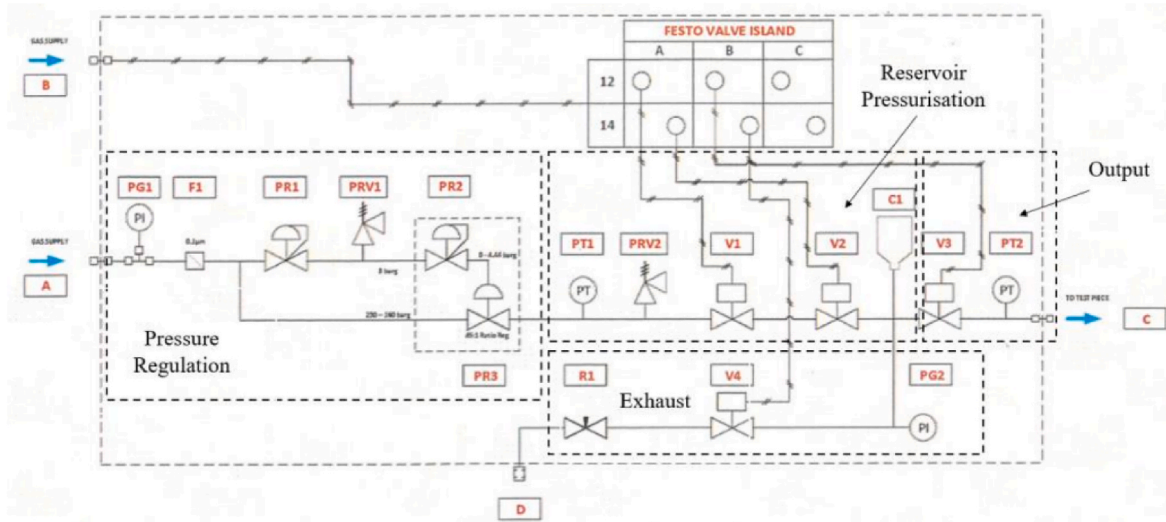
Fig. 5. Cyclic pressure test equipment.
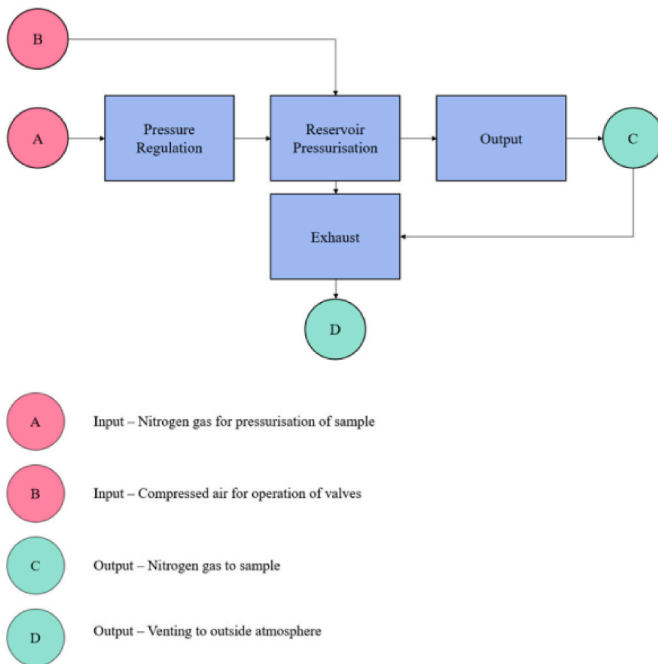
Fig. 6. Flow diagram of pressure testing rig subsystems.

Table 2
Purpose and operation of subsystems within pressure test rig.

Subsystem	Purpose	Operation
Pressure Regulation	Regulates pressure supplied to reservoir	A pressure regulator is used to ensure constant pressure is fed into the sample, even if the upstream pressure from the input varies.
Reservoir Pressurisation	Incrementally pressurise reservoir prior to output to sample	The regulated gas supply is used to incrementally pressurise the reservoir prior to release to sample.
Output	Output of pressure to sample	Pressurised gas is released to the sample via output C.
Exhaust	Output of pressure to surroundings	Pressurised gas leaves the sample via the exhaust, output D.

joint. Some joints also contained a large number of smaller pores, or voids, across the joint area, such as those seen in Fig. 7d and f.

These observations are significant, as larger voids are known to directly affect the mechanical strength of a joint due to a reduction in solder area [45], whereas smaller pores that exist close to one another may have a higher tendency to cause crack propagation across the joint [46].

4.2. Stress 1

The first stage of the SSALT, or S1, was to expose the sample to 500 cycles of internal pressure loading between 0 and 65 bar. Each cycle took between 45s and 1 min to complete.

The sample was able to withstand 500 cycles of this internal pressure loading, with no drop in the pressure that could be held by the sample. XCT data was collected for the joints similarly to pre-testing, in order to understand if any changes to the joints, or voids, could be seen within the sample. Comparisons of two joints before and after this first stage of loading can be seen in Fig. 8. The differences in colour/contrast between the before and after images are due to differences in scanning and postprocessing, and not indicative of a change within the sample.

As can be seen in Fig. 8, there was no noticeable difference in the structure of the joints nor the size and shape of the porosity contained within the joints. Two joints were compared, one with several smaller pores within the joint, Fig. 8a, and one with a significantly larger pore, Fig. 8b. In neither case did the voids change shape or size, nor was there any indication of cracking or failure within the joints.

4.3. Stress 2

The next stage of the SSALT was to increase the cyclic loading from 0 - 65 bar to 0–85 bar. The number of cycles remained the same at 500 cycles. The sample was again able to withstand the entire 500 cycle test with no drop in pressure that the sample was able to withstand. As in the case of previous stress levels, the sample was XCT scanned to investigate the inner structure of the joints. Here, significant changes could be seen within the joints compared to the previous iteration. The first joint in which significant changes could be seen is presented in Fig. 9.

As can be seen from Fig. 9, the joint had a singular large void and many smaller voids within the joint prior to any testing, Fig. 9a. However, after the S_2 stage of the SSALT, a crack can be seen that propagates from the large void, through some of the smaller voids, Fig. 9b. This indicates that the sample experienced changes to the structure of the joint during the internal pressure cycling, even though no change to the
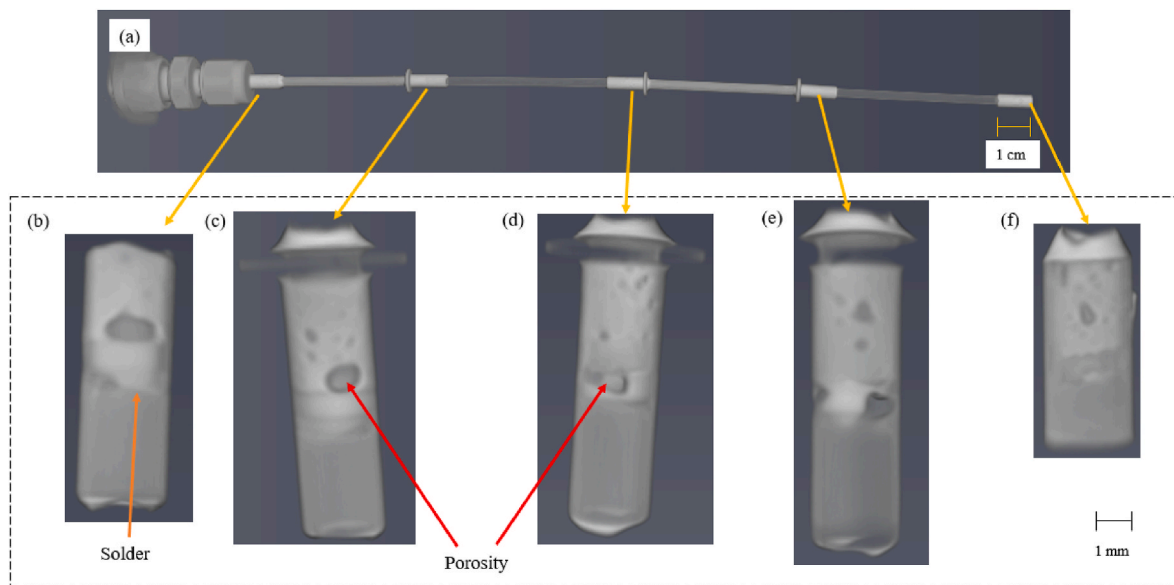
Fig. 7. XCT imaging of sample prior to pressure testing (a), with solder sections of individual joints highlighted in greater detail (b)–(f).
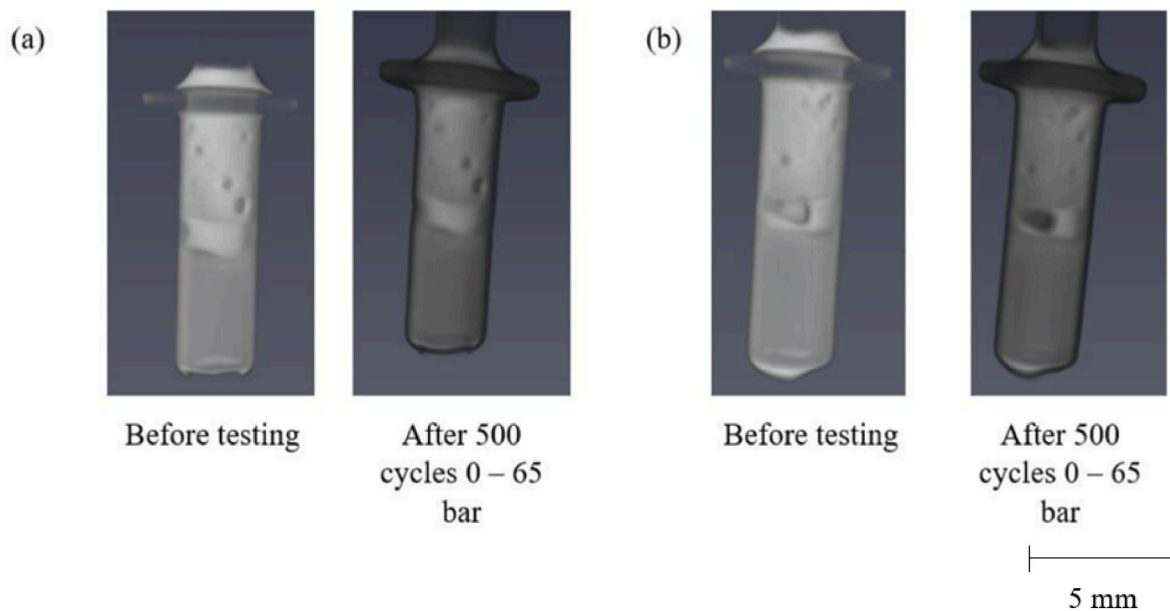
Fig. 8. XCT images of two joints before and after cyclic pressure testing at 500 cycles 0–65 bar loading.

performance of the sample was indicated during the testing process.

As can be seen in Fig. 10, other joints within the sample also displayed significant changes within the solder material after S_1 and S_2 stress cycles. Crack propagation radially across a joint circumference was seen as shown in Fig. 10a, as well as a larger bulk failure of material, Fig. 10b. In each case, cracks seem to appear either from, or close to, where voids already existed within the joint prior to testing. It can therefore be assumed that voids cause a stress concentration during cyclic loading and can provide a seed for failure of the material.

4.4. Stress 3

The final stage of the SSALT programme, S3, was to expose the sample to 500 cycles of internal pressure loading, from 0 to 130 bar.

However, upon pressurising the sample it was seen that the sample could only withstand a maximum load of 111 bar. After this pressure

which no additional pressure could be achieved as the leak rate was approximately equal to the input flow rate of the rig (Fig. 11). Accordingly, the S3 design pressure of 130 bar was not achieved.

The loss in pressure after the sample reaches 111 bar was then isolated in order to calculate the leak rate, which was found to be 0.19 bar per second. This rate of pressure drop was sufficient to ensure that the sample could not hold any additional pressure. The incremental nature of the pressurisation system means that at each pressure increment a minor over pressurisation is recorded due to the dynamic pressure wave hitting the sensor. This is observed even at low pressures or in fully sealed samples. However, as shown in Fig. 11 there is an observable reduction in pressure at pressures higher than 75 bar. This demonstrates that the sample displayed failure at lower pressures. Despite this pressure drop, the sample could withstand further loading up to a maximum pressure of 111 bar, at which point the leak rate approximately equalled the inflow rate of the sample.
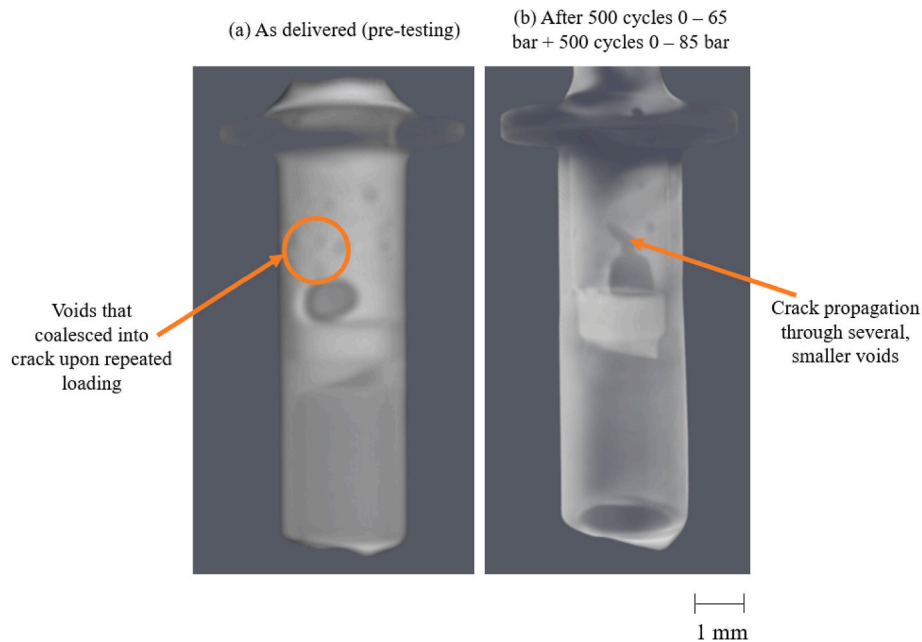
Fig. 9. Joint before (a) and after (b) testing to S_1 and S_2 cycles of SSALT, with significant changes to voids seen after testing.
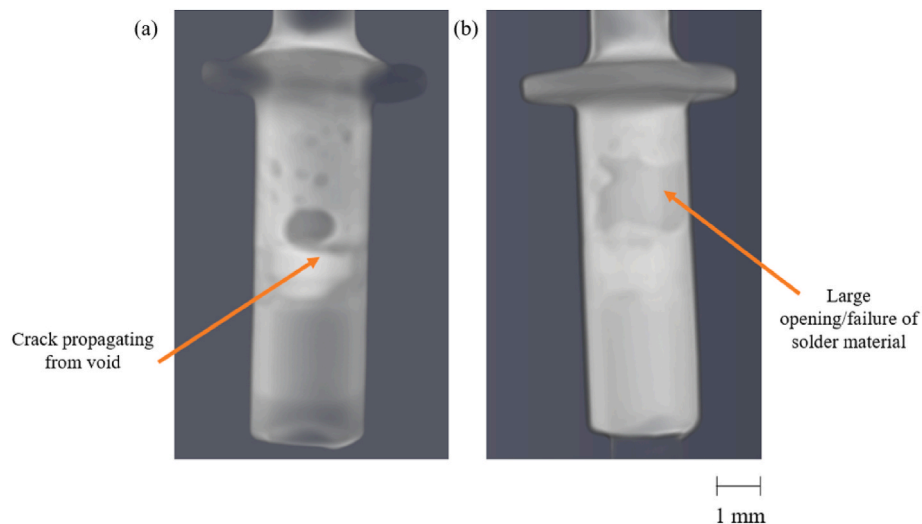
Fig. 10. Failures within other joints after S_1 and S_2 stress cycles, including crack propagation from voids (a) and large opening/failure of solder material, (b).

Quantification of the leak rate was attempted at each of the pressure holds, however the design of the rig (and SSALT programme) meant that few data points were collected at each pressure. This limited data set, in combination with the noise of the pressure sensor meant that for pressures below 111 bar the confidence interval was greater than the magnitude of the estimate, which ensured that no meaningful results could be obtained. On this basis, leak rate analysis was performed only at 111 bar.

In accordance with the SSALT programme, a failure to reach the S3 means that the testing schedule can be considered completed. However, further loading provides insights into subsequent failure modes. For this reason, the sample was not modified or fixed, but was instead cyclically tested between 0 and 100 bar for 500 cycles, rather than the initially planned 0–130 bar. In order to investigate the progression of failure during these 500 cycles, the pressure loss at 100 bar maximum pressure was determined at 50 cycle increments, as shown in Fig. 12.

As can be seen from Fig. 12, the pressure loss when the sample is loaded to ~100 bar maximum pressure is initially around 0.19 bar/s,

and this rises to just under 0.45 bar/s after 500 cycles. It can also be seen between 0 and 350 cycles, the pressure loss is fairly consistent, with a large rise seen at 400 cycles. The leak rate then continues to rise until the end of the testing schedule. This implies that further failures to the samples occurred around 400 cycles, which continued to grow/worsen upon further loading. However, it should also be noted that even after 500 cycles, the sample was still able to be pressurised up to 100 bar by the test rig, despite the increase in the leak rate. Due to the early failure of the sample and the lack appropriate model to accommodate for this associated under pressure, the results could not be extrapolated to the likely performance of the sample under normal operational conditions.

4.5. Post-testing analysis

After the final cycle of testing, the samples were mounted in resin and polished, such that the cross sections of the joints could be studied using OM. During investigation, it could be seen that failures in the solder could be seen across various samples. Fig. 13 shows a failure that
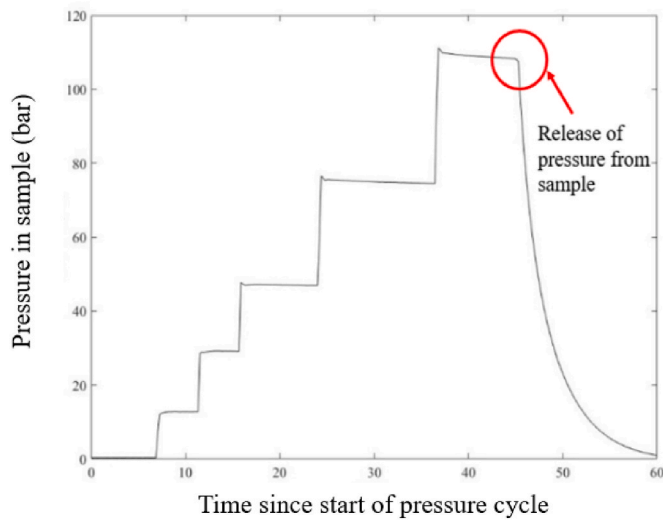
Fig. 11. Pressurisation of sample to 111 bar.
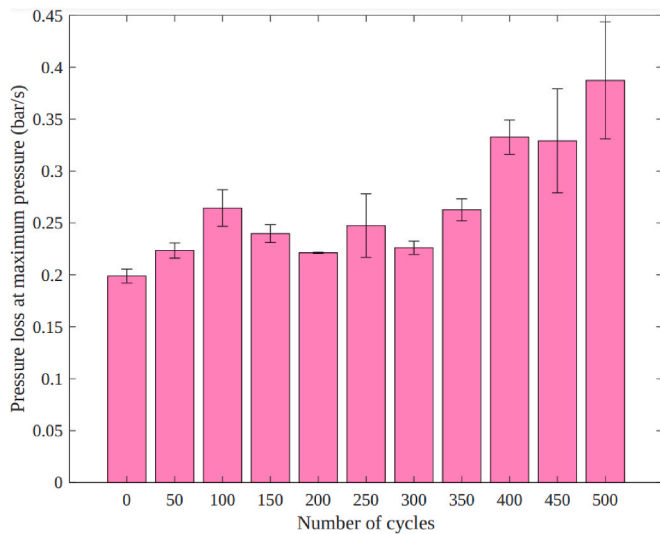
Fig. 12. Pressure loss at maximum 100 pressure, as recorded after n number of cycles, per 50 cycle increments.

Fig. 13. Cross section of soldered joint after lifetime testing (a), with a significant failure in the solder present (b).

could be seen within the soldered section of a joint after lifetime testing.

As can be seen from Fig. 13a a longitudinal void around 0.66 mm in total length was present within the solder of the joint. Upon closer inspection, Fig. 13b, it can be seen that several dark narrow features indicative of channels or cracks are present within the solder. These are connected to a larger dark feature on the left-hand side. The application of pressure within the pipes has likely resulted in the growth and amalgamation of these cracks into this larger feature, as this would be the most energetically favourable solution to the application of stress. Similar sized voids were also seen on other samples, Fig. 14.

As can be seen from both Fig. 14a and b, after lifetime testing, samples tend to have large voids present within the solder, with the remaining solder appearing largely intact. This corresponds with the XCT data collected before and after testing, which implied that cracks and failures occurred from voids present within the sample before testing, and that cracks do not spontaneously appear within the solder. Therefore, it can be assumed that the voids seen in Fig. 14 were present prior to commencing lifetime testing, however lifetime testing likely exacerbated the voids either by enlarging them, or causing crack propagation through the surrounding solder.

5. Discussion

During the lifetime testing of this sample, which was formed of a series of 10 soft soldered and vacuum brazed joints, it could be seen that after 500 cycles of 0–65 bar internal pressure, and then a further 500 cycles of 0–85 bar pressure, the sample had developed significant leaks which would not allow it to hold pressure above 111 bar.

This resulted in the final planned stage of the SSALT unable to be completed, which would have seen the sample tested to 500 cycles of 0–130 bar pressure loading.

While none of the joints within the sample suffered a catastrophic failure, i.e., a failure which resulted in an inability to hold any internal pressure, progressive failures caused samples to develop leaks which worsened in magnitude at higher pressures. A maximum leak rate of 0.44 bar/s was recorded at the end of testing, when a sample was loaded to 100 bar internal pressure. Such a pressure loss would be significantly detrimental to the operation of the components in service.

Upon inspection of the joints using XCT and OM, it could be seen that failures were limited to the soldered sections of the joints, with the vacuum brazed joints remaining intact after testing. It could also be seen that cracks propagated from existing voids within the solder after cyclic loading, with cracks propagating between voids to form a larger flaw.

This is significant as it implies that voids within the solder can cause early failures during cyclic pressure loading, and such failures could be avoided by minimising voids during the joining process. It can also be assumed that while porosity may not impact the ability of the sample to
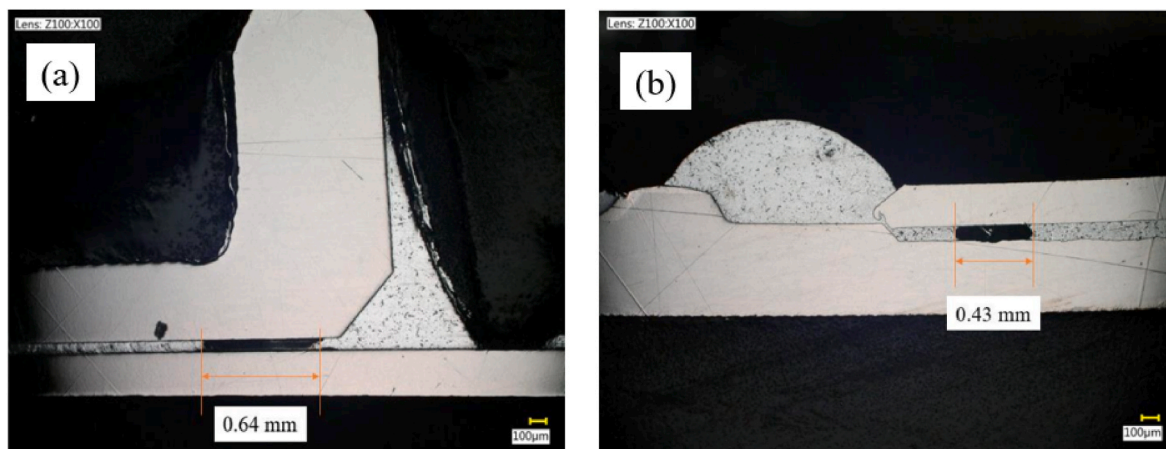
Fig. 14. Sample with a 0.64 mm void (a) and 0.43 mm void (b) within a soldered joint after lifetime testing.

hold pressure without leaks prior to cyclic loading, as evidenced by the fact the sample could withstand a 186 bar pressure prior to testing, porosity can then lead to early failure. In turn, this shows that simply testing the joints by a single pressurisation is not sufficient to determine the quality or lifetime performance of such a joint and non-destructive testing (NDT) or internal inspections of the solder should be carried out for critical parts in order to characterise the porosity within the solder.

The results from this study, and the insights gained, show that cyclic testing is a valuable tool in analysing the performance of parts that will experience internal pressure loading over their lifetime.

6. Conclusions

This work has demonstrated that components that will experience internal, cyclic pressure loading during service should be qualified using a representative lifetime testing model. This is due to the fact that some failures due to internal pressure loading cannot be determined using other forms of testing such as pressure loading to a set value, or destructive testing of samples.

A custom piece of equipment with a control system that allows automated testing over a long period of time was built to serve this purpose. The equipment and code created to carry out the SSALT on such parts demonstrate proof of concept, that such tests can be feasibly carried out and insightful results gained.

Progressive failures were seen within soldered samples, where crack propagation was initiated from areas of existing porosity in the 'as delivered' state. Crack propagation was seen both from larger voids within the solder, as well as propagation of cracks through several, smaller pores. Further work is necessary to determine the effect of porosity size, shape and relative location on crack propagation under cyclic internal pressure loading.

This work has demonstrated the importance of non-destructively analysing thin-walled cooling pipe connections prior to their installation and service. This can be used to estimate the likely impact of porosity on part performance during a single loading cycle via features such as pore diameter. However, the long-term cyclic behaviour remains challenging to predict due to presence of pores with multiple sizes and spacing in real samples.

Funding

Declaration of competing interest

The authors declare that they have no known competing financial interests or personal relationships that could have appeared to influence the work reported in this paper.

References

[1] McNair SAM, et al. Manufacturing technologies and joining methods of metallic thin-walled pipes for use in high pressure cooling systems. Int J Adv Des Manuf Technol 2022;118(3):667–81. https://doi.org/10.1007/s00170-021-07982-8. 2022/01/01.

[2] Hartl C. Review on advances in metal micro-tube forming. Metals 2020;9(5). https://doi.org/10.3390/met9050542.

[3] Yi Y, Komine H, Furushima T. Effect of forming conditions on microstructure and room-temperature mechanical characterization of Zn–22Al superplastic microtubes fabricated by direct extrusion. Mater Sci Eng, A 2022;844:143160. https://doi.org/10.1016/j.msea.2022.143160. 2022/06/02.

[4] Ahamed MS, Saito Y, Mashiko K, Mochizuki M. Characterization of a high performance ultra-thin heat pipe cooling module for mobile hand held electronic devices. Heat Mass Tran 2017;53(11):3241–7. https://doi.org/10.1007/s00231-017-2022-7. 2017/11/01.

[5] Chen X, Ye H, Fan X, Ren T, Zhang G. A review of small heat pipes for electronics. Appl Therm Eng 2016;96:1–17. https://doi.org/10.1016/j.applthermaleng.2015.11.048. 2016/03/05/.

[6] Yu H, Li J, He Z. Formability assessment of plastic joining by compression instability for thin-walled tubes. Int J Adv Des Manuf Technol 2018;97(9):3423–30. https://doi.org/10.1007/s00170-018-2128-1. 2018/08/01.

[7] Bhadeshia H, Honeycombe R. Chapter 13 - weld microstructures. In: Bhadeshia H, Honeycombe R, editors. Steels: microstructure and properties. fourth ed. Butterworth-Heinemann; 2017. p. 377–400.

[8] Runesson K, Skyttebol A, Lindgren LE. 3.05 - nonlinear finite element analysis and applications to welded structures. In: Milne I, Ritchie RO, Karihaloo B, editors. Comprehensive structural integrity. Oxford: Pergamon; 2003. p. 255–320.

[9] Cooke KO. 9 - a comparative analysis of techniques used for joining intermetallic MMCs. In: Mitra R, editor. Intermetallic matrix composites. Woodhead Publishing; 2018. p. 221–41.

[10] Hebda M, Kaczor P, Miernik K. Vacuum brazing of stainless steel depending on the surface preparation method and temperature of the process. Arch Metall Mater 2019;64:5–11. https://doi.org/10.24425/amm.2019.126210. 03/01.

[11] Behúlová M, Vrtiel Š, Nagy M. Induction brazing of thin-walled pipes from AISI 304 steel using copper-based solder. IOP Conf Ser Mater Sci Eng 2019;465(1):012001. https://doi.org/10.1088/1757-899X/465/1/012001. 2019/01/01.

[12] BS EN ISO 13919-2:2021 Electron and laser-beam welded joints. Requirements and recommendations on quality levels for imperfections. Aluminium, magnesium and their alloys and pure copper. 2021.

[13] BS EN ISO 5817:2023 TC Welding. Fusion-welded joints in steel, nickel, titanium and their alloys (beam welding excluded). Quality levels for imperfections; 2023.

[14] BS EN ISO 13919-2:2021 Electron and laser-beam welded joints. Requirements and recommendations on quality levels for imperfections - aluminium, magnesium and their alloys and pure copper. 2021.

[15] McNair SAM, Srisuriyachot J, Omole S, Connolley T, Rhead A, Lunt AJG. The effect of porosity on strain evolution and failure of soldered, small-diameter, thin-walled metallic pipes. J Mater Res Technol 2023;22:2409–24. https://doi.org/10.1016/j.jmrt.2022.12.088. 2023/01/01/.

[16] Bing K, Eigenmann B, Scholtes B, Macherauch E. Brazing residual stresses in components of different metallic materials. Mater Sci Eng, A 1994;174(1):95–101. https://doi.org/10.1016/0921-5093(94)91116-9. 1994/01/01/.

[17] Karamanos S. Chapter 5 - mechanical behavior of metal pipes under internal and external pressure. In: Karamanos S, editor. Structural mechanics and design of metal pipes. Elsevier; 2023. p. 133–86.

[18] Thomas GO. The response of pipes and supports to internal pressure loads generated by gaseous detonations. J Pressure Vessel Technol 2001;124(1):66–73. https://doi.org/10.1115/1.1427342.

[19] Robertson A, Li H, Mackenzie D. Plastic collapse of pipe bends under combined internal pressure and in-plane bending. Int J Pres Ves Pip 2005;82(5):407–16. https://doi.org/10.1016/j.ijpvp.2004.09.005. 2005/05/01/.

[20] Amaya-Gómez R, Sánchez-Silva M, Bastidas-Arteaga E, Schoefs F, Muñoz F. Reliability assessments of corroded pipelines based on internal pressure – a review. Eng Fail Anal 2019;98:190–214. https://doi.org/10.1016/j.engfailanal.2019.01.064. 2019/04/01/.

[21] Song P, Lawrence D, Keane S, Ironside S, Sutton A. Pressure cycling monitoring helps ensure the integrity of energy pipelines. International Pipeline Conference 2010;44205:583–7.

[22] Borodii MV, Adamchuk MP, Stryzhalo VO, Yaskovets' ZS. Experimental study on cyclic creep of pipes. Strength Mater 2022;54(3):378–86. https://doi.org/10.1007/s11223-022-00413-3. 2022/05/01.

[23] Singh N, Das S, Song P, Yoosef-Ghodsi N. Numerical investigation of pressure-cycling-induced fatigue failure of wrinkled energy pipelines. J Offshore Mech Arctic Eng 2021;144(1). https://doi.org/10.1115/1.4051545.

[24] Pinheiro BdC, Pasqualino IP. Fatigue analysis of damaged steel pipelines under cyclic internal pressure. Int J Fatig 2009;31(5):962–73. https://doi.org/10.1016/j.ijfatigue.2008.09.006. 2009/05/01/.

[25] Shoheib MM, Shahrooi S, Shishehsaz M, Hamzehei M. Fatigue crack propagation of welded steel pipeline under cyclic internal pressure by bézier extraction based XIGA. J Pipeline Syst Eng Pract 2022;13(2):04022001. https://doi.org/10.1061/(ASCE)PS.1949-1204.0000633.

[26] Dmytryk VV, Glushko AV, Poznyakov VD, Kasyanenko IV. Creep pores in welded joints of steam pipelines. Strength Mater 2023;55(2):287–95. https://doi.org/10.1007/s11223-023-00523-6. 2023/03/01.

[27] Fard N, Li C. Optimal simple step stress accelerated life test design for reliability prediction. J Stat Plann Inference 2009;139(5):1799–808. https://doi.org/10.1016/j.jspi.2008.05.046. 2009/05/01/.

[28] Nelson W. Accelerated life testing - step-stress models and data analyses. IEEE Trans Reliab 1980;R-29:103–8.

[29] Tang L-C. Multiple-steps step-stress accelerated life test. In: Pham H, editor. Handbook of reliability engineering. London: Springer London; 2003. p. 441–55.

[30] Stachon K, et al. Modern high-availability multi-stage power distribution system for the CMS phase-2 upgrade. J Instrum 2023;18(2):C02053. https://doi.org/10.1088/1748-0221/18/02/C02053. 2023/02/23.

[31] J. Contardo DK, Mans M, Silvestris J, Butler L. Technical proposal for the phase-II upgrade of the CMS detector. 2015. CERN-LHCC-2015-010 ; LHCC-P-008 ; CMS-TDR-15-02

[32] BS EN ISO 4126-2:2019: safety devices for protection against excessive pressure: bursting disc safety devices. British Standards Institute; 2019.

[33] Feld L, Karpinski W, Merz J, Wlochal M. CO2 cooling for the CMS tracker at SLHC. J Instrum 2011;6(1):C01091. https://doi.org/10.1088/1748-0221/6/01/C01091. 2011/01/19.

[34] Daguin J, et al. Evaporative CO2 cooling system for the upgrade of the CMS pixel detector at CERN. In: 13th InterSociety conference on thermal and thermomechanical phenomena in electronic systems; 2012. p. 723–31. https://doi.org/10.1109/ITHERM.2012.6231499. 30 May-1 June 2012.

[35] Arling J-H, Gregor I-M. Material budget imaging with multi-GeV electrons - calibration and applications for 2D material scanning. J Phys Conf 2022;2374(1):012007. https://doi.org/10.1088/1742-6596/2374/1/012007. 2022/11/01.

[36] Migliore E. CMS Tracker alignment and material budget measurements. PoS 2011;RD11. https://doi.org/10.22323/1.143.0008. 003.

[37] Roy Chowdhury S. Estimation of the material budget of the CMS Tracker using the triplet method. PoS 2021;ICHEP2020:776. https://doi.org/10.22323/1.390.0776.

[38] Cheng L, Ribatski G, Thome JR. Two-phase flow patterns and flow-pattern maps: fundamentals and applications. Appl Mech Rev 2008;61(5). https://doi.org/10.1115/1.2955990.

[39] Kandlikar SG. Fundamental issues related to flow boiling in minichannels and microchannels. Exp Therm Fluid Sci 2002;26(2):389–407. https://doi.org/10.1016/S0894-1777(02)00150-4. 2002/06/01/.

[40] Fukano T, Kariyasaki A. Characteristics of gas-liquid two-phase flow in a capillary tube. Nucl Eng Des 1993;141(1):59–68. https://doi.org/10.1016/0029-5493(93)90092-N. 1993/06/02/.

[41] Ullmann A, Brauner N. The prediction of flow pattern maps in minichannels. Multiphas Sci Technol 2007;19:49–73. https://doi.org/10.1615/MultScienTechn.v19.i1.20. 01/01.

[42] Pantazică M, Svasta P, Wohlrabe H, Wolter KJ. Factors influencing the formation of voids in chip component solder joints. In: 2013 IEEE 19th international symposium for design and technology in electronic packaging (SIITME); 2013. p. 277–82. https://doi.org/10.1109/SIITME.2013.6743690. 24-27 Oct. 2013.

[43] Cheng S, Huang C-M, Pecht M. A review of lead-free solders for electronics applications. Microelectron Reliab 2017;75:77–95. https://doi.org/10.1016/j.microrel.2017.06.016. 2017/08/01/.

[44] Otiaba KC, Okereke MI, Bhatti RS. Numerical assessment of the effect of void morphology on thermo-mechanical performance of solder thermal interface material. Appl Therm Eng 2014;64(1):51–63. https://doi.org/10.1016/j.applthermaleng.2013.12.006. 2014/03/01/.

[45] Xinmeng Z, et al. Effect of soldering temperature on the reliability of Sn-Ag-Cu lead-free solder joints. J Electron Mater 2021;50(3):869–80. https://doi.org/10.1007/s11664-020-08715-5. 2021/03/01.

[46] Yunus M, Primavera A, Srihari K, Pitarresi JM. Effect of voids on the reliability of BGA/CSP solder joints. In: Twenty sixth IEEE/CPMT international electronics manufacturing technology symposium (cat. No.00CH37146); 2000. p. 207–13. https://doi.org/10.1109/IEMT.2000.910730. 3-3 Oct. 2000.

[47] Ahat S, Du L, Sheng M, Luo L, Kempe W, Freytag J. Effect of aging on the microstructure and shear strength of SnPbAg/Ni-P/Cu and SnAg/Ni-P/Cu solder joints. J Electron Mater 2000;29(9):1105–9. https://doi.org/10.1007/s11664-004-0272-x. 2000/09/01.

[48] Laurila T, Vuorinen V, Mattila T, Kivilahti JK. Analysis of the redeposition of AuSn4 on Ni/Au contact pads when using SnPbAg, SnAg, and SnAgCu solders. J Electron Mater 2005;34(1):103–11. https://doi.org/10.1007/s11664-005-0186-2. 2005/01/01.

[49] Ming L, Lee KY, Olsen DR, Chen WT, Tan BTC, Mhaisalkar S. Microstructure, joint strength and failure mechanisms of SnPb and Pb-free solders in BGA packages. IEEE Trans Electron Packag Manuf 2002;25(3):185–92. https://doi.org/10.1109/TEPM.2002.801649.

[50] Parsey JM, Valocchi S, Cronin W, Mohr J, Scrivner BL, Kyler K. A metallurgical assessment of SnPbAg solder for GaAs power devices. JOM 1999;51(3):28–31. https://doi.org/10.1007/s11837-999-0024-8. 1999/03/01.

[51] Lee KY, Li M. Formation of intermetallic compounds in SnPbAg, SnAg, and SnAgCu solders on Ni/Au metallization: physical metallurgical and materials science (in English) Metall Mater Trans Oct 2001;32A(10):2666. 2023-07-05 2001. [Online]. Available: https://www.proquest.com/scholarly-journals/formation-intermetallic-compounds-snpbag-snag/docview/213709855/se-2?accountid=14116. https://suprimo.lib.strath.ac.uk/openurl/SU/SUVU01?genre=article&atitle=Formation+of+intermetallic+compounds+in+SnPbAg%2C+SnAg%2C+and+SnAgCu+solders+on+Ni%2FAu+metallization%3A+Physical+Metallurgical+and+Materials+Science&author=Lee%2C+K+Y%3BM+Li&volume=32A&issue=10&spage=2666&date=2001-10-01&rft.btitle=&rft.jtitle=Metallurgical+and+Materials+Transactions&issn=1073-5623&isbn=&sid=ProQ%3Asciencejournals.

[52] Struers. Metallographic Preparation of Stainless Steel. https://www.struers.com/en/Knowledge/Materials/Stainless-Steel#; 2023.